Supporting Information

Mesoporous Al$_2$O$_3$ zincophilic sieve enables ultra-long lifespan of Zn-ion batteries

Qianyao Wu, [a] Kaiwen Qi, [a] Mengke Liu, [a] Zhechen Fan, [a] Xuan Ding, [a] Shiyuan Chen, [a] and Yongchun Zhu*[a]

[a]Department of Applied Chemistry

University of Science and Technology of China

Hefei 230026, P. R. China

*Corresponding authors:

E-mail: ychzhu@ustc.edu.cn

Material synthesis processes

Preparation of different pore size of mesoporous Al$_2$O$_3$ powder: LA-MA was prepared according to previous reports.[1] All chemicals were used directly without purification and bought from Macklin. Aqueous solutions of Al(NO$_3$)$_3$ 9H$_2$O, carboxylic acid and triethanolamine (TEA) with a molar ratio of 1:0.1:3 were mixed to create the precursors. Al (NO$_3$)$_3$ 9H$_2$O (14.716 g) was dissolved in water (20 mL) and warmed at 80 °C to make an aqueous solution of aluminum nitrate. The mixture of lactic acid (0.36 g) and TEA (16 mL) was dissolved in water (30 mL) to get a clear solution. At 80°C, this mixture was then added into aluminum nitrate solution to produced white precipitate. After that, the reaction mixture was stirred for 12 hours at room temperature and then transferred into the teflon container and aged for 24 hours at 90 °C. After filtering, the precursor powder is created by washing with distilled water and drying at 90 °C. After that, the precursor was calcined for three hours in air at 550 °C to produce porous alumina powder. Lactic acid was substituted for other carboxylic acids such as lauric acid, hexanoic acid and stearic acid. Alumina formed by reacting just with aluminum nitrate and TEA is known as MA, while alumina prepared

by reacting with stearic acid, lauric acid, hexanoic acid and lactic acid are referred to C18-MA, C12-MA, C6-MA and LA-MA, respectively.

Preparation of LA-MA@Zn layer: The obtained LA-MA and PVDF powder were mixed at the radio of 9:1, and then add appropriate amount of N-methyl pyrrolidone solvent. The slurry was cast onto Zn foil after 12 hours of ball milling, and dried at 60°C for 12 hours in vacuum.

Cathode preparation: According to previous reports,[2] CNT/MnO_2 composite cathode material was obtained. A mixture of 70wt% CNT/MnO_2 powder, 20wt% Ketjenblack, 10wt% PVDF and several droplets of NMP was used to create the CNT/MnO_2 cathode. The slurry is poured onto titanium mesh and dried in vacuum for 12h at 60°C.

Material characterization

X-ray diffraction (XRD) experiments were performed using Cu Kα (λ=1.54182Å) radiation on a Philips X'Pert Super diffractometer. Scanning electron microscopy (SEM, Zeiss Gemini 450) image and transmission electron microscopy (TEM, Hitachi H7650.) were used to characterized the surface morphologies of samples. The Brunauere–Emmette–Teller (BET) specific surface and pore size distributions of samples were measured by using a Micromeritics Tristar II 3020 instrument. FT-IR were tested on Hyperion 3000 system. A Thermo ESCALAB 250 X-ray photoelectron spectrometer (Perkin-Elmer) was used to collect X-ray photoelectron spectroscopy (XPS). Raman spectra were performed by a HORIBA LabRAM HR Evolution Invia confocal laser micro-Raman spectrometer at 733 nm.[3] Atomic force microcope (AFM) images were obtained by NanoScope IIIa (Bruker, USA).

Electrochemical measurements

CR2016 coin cells with a glass fiber separator (Whatman, GF/C) and $ZnSO_4$ (2 M) electrolyte were used to measure the electrochemical performance of symmetric cells and half cells. And full cell used $ZnSO_4$ (2 M) + $MnSO_4$ (0.2 M) as electrolyte and CNT/MnO_2 as cathode. The performance of the galvanostatic charge/discharge was evaluated by NEWARE CT4008T and LAND CT2001A. The electrochemical impedance spectroscopy (EIS), linear sweep voltammetry (LSV), Tafel plots, chronoamperometry (CA) and cyclic voltammetry (CV) were tested on a CHI 660E electrochemical workstation. The frequency range of EIS is 100KHz to 1Hz. And the voltage window of CV is 0.8-1.8V.
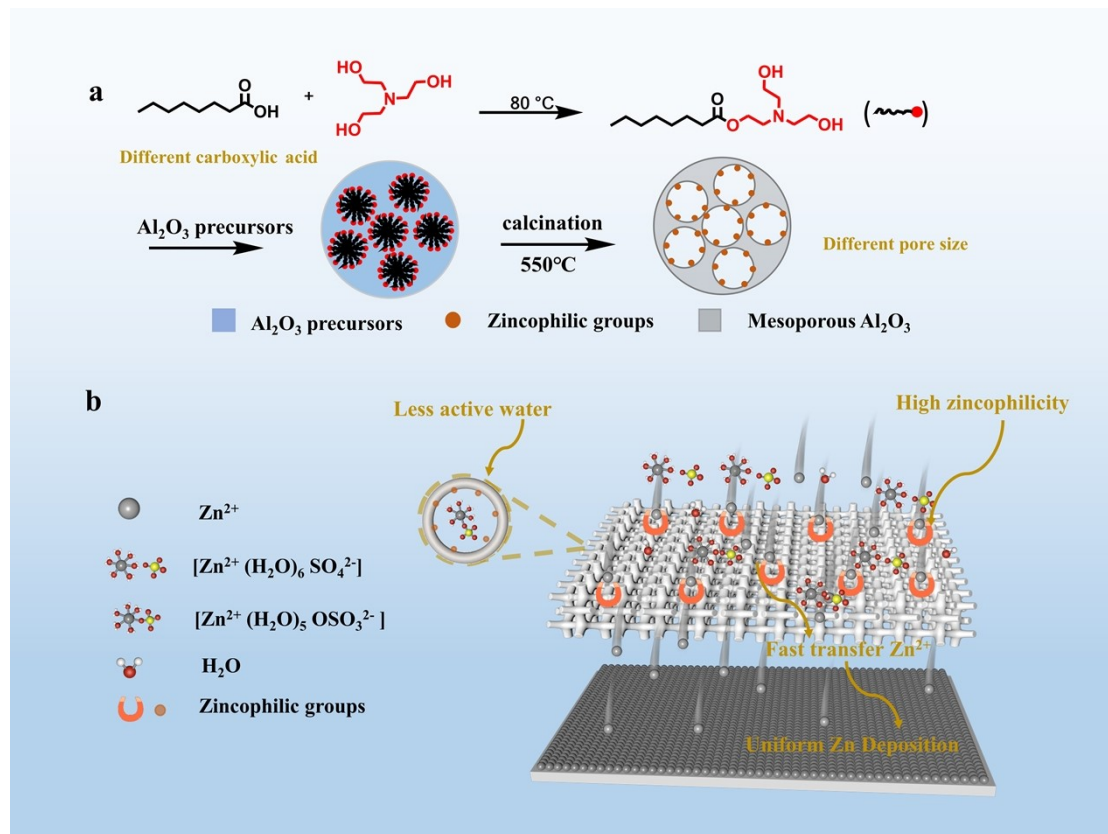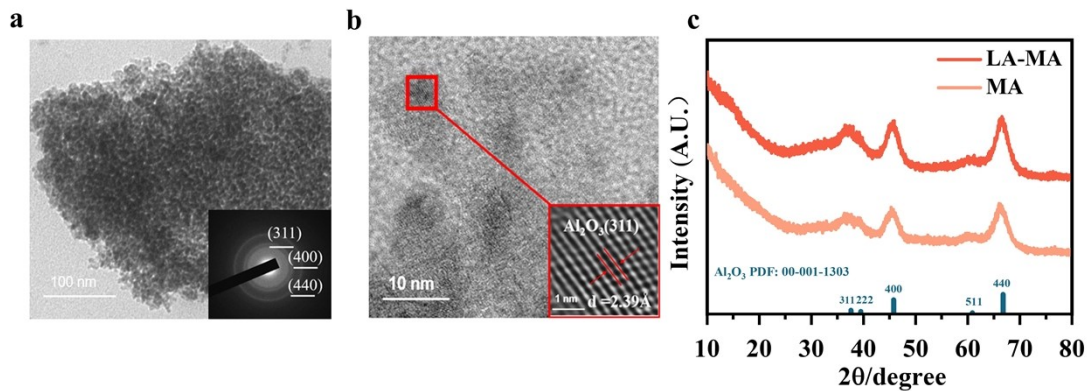
Fig. S1 Diagrams of (a) synthesis mechanism of different pore sizes mesoporous Al_2O_3 with zincophilic groups and (b) Zn deposition behavior on LA-MA@Zn anode.
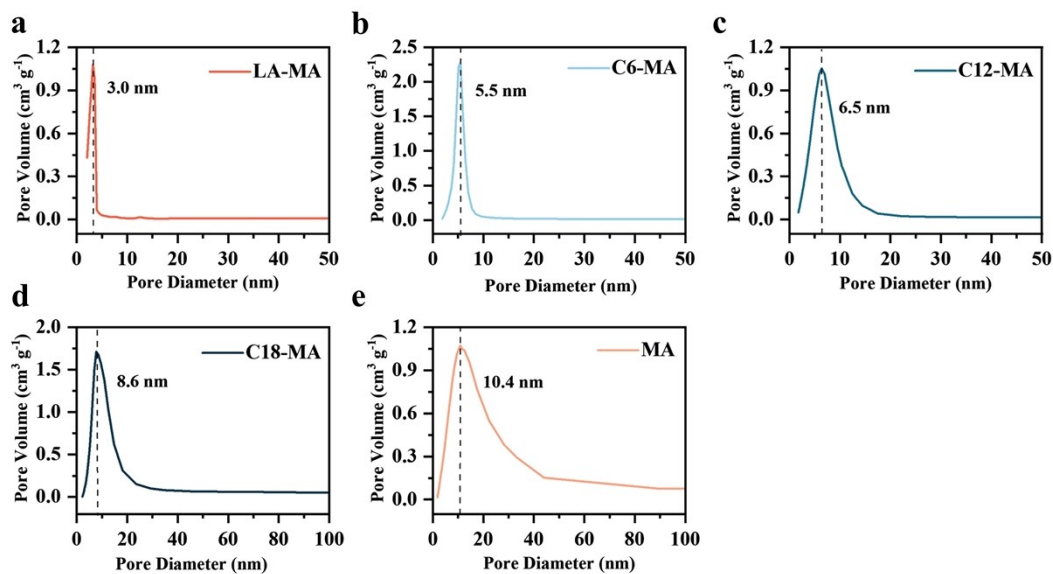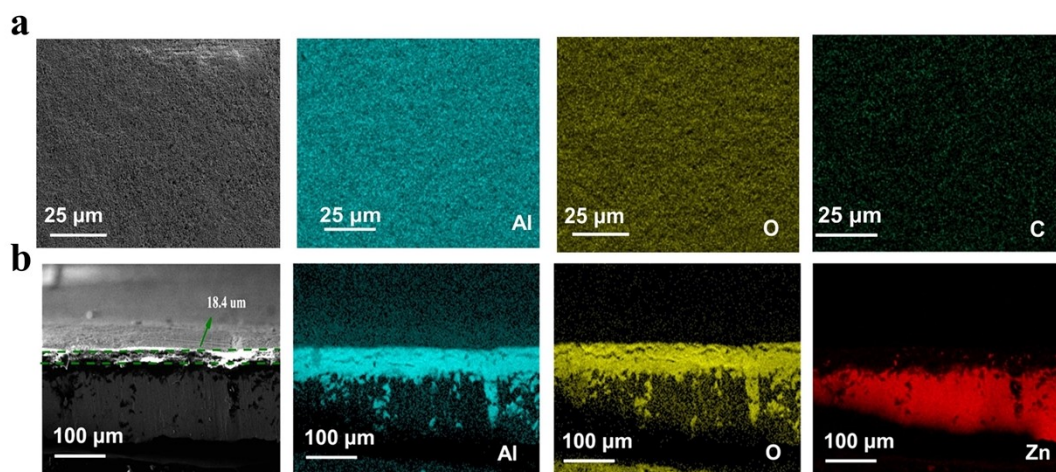
Fig. S2 Pore-size distribution of (a) LA-MA, (b) C6-MA, (c) C12-MA, (d) C18-MA, (e) MA powder.
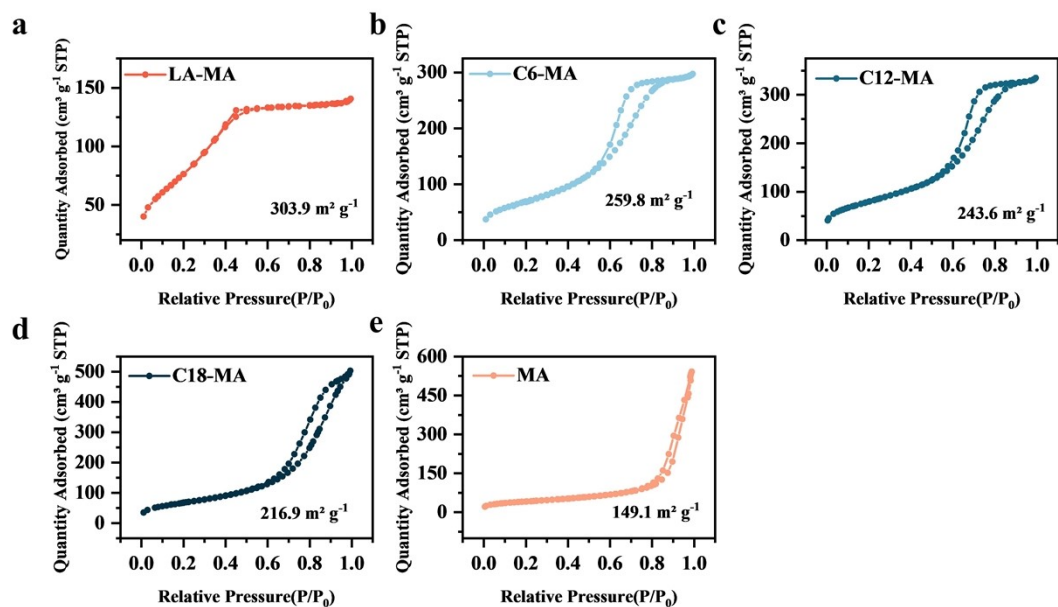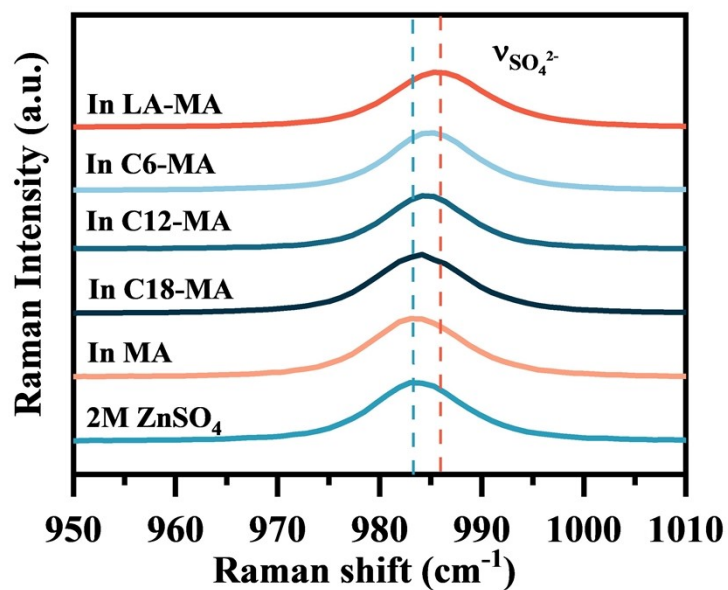

Fig. S3 Nitrogen adsorption/desorption isotherm plots of (a) LA-MA, (b) C6-MA, (c) C12-MA, (d) C18-MA, (e) MA powder.
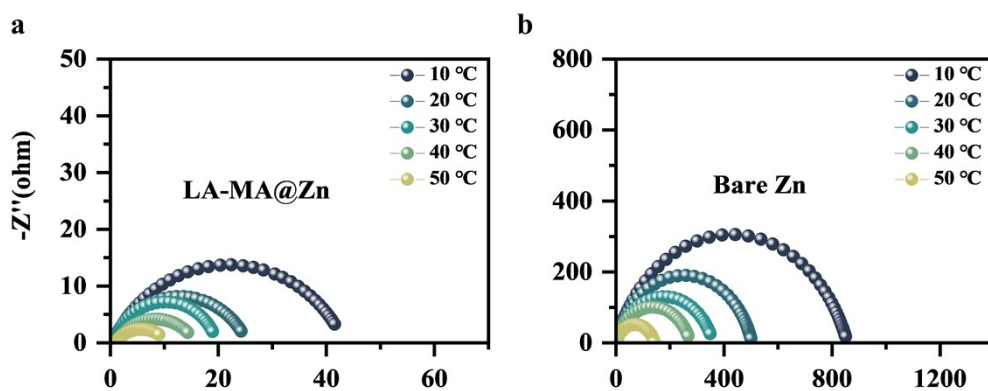
Fig. S4 (a) TEM images and corresponding SAED pattern, (b) HRTEM images, (c) XRD patterns of LA-MA powder.
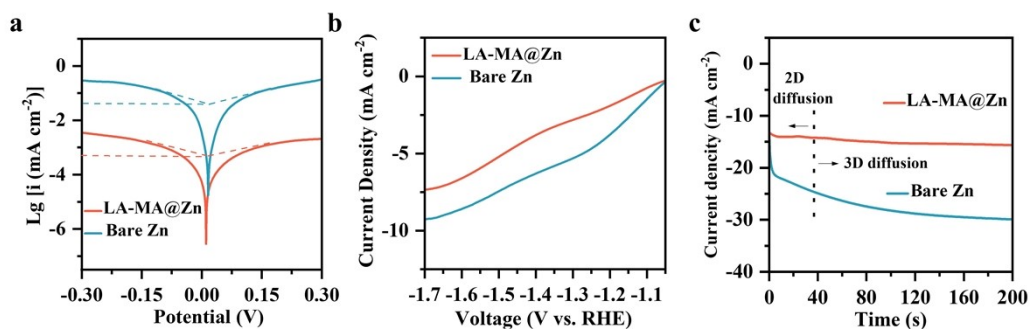

Fig. S5 SEM images and EDS mapping images of (a) LA-MA@Zn surface, (b) the cross-sectional of LA-MA@Zn.
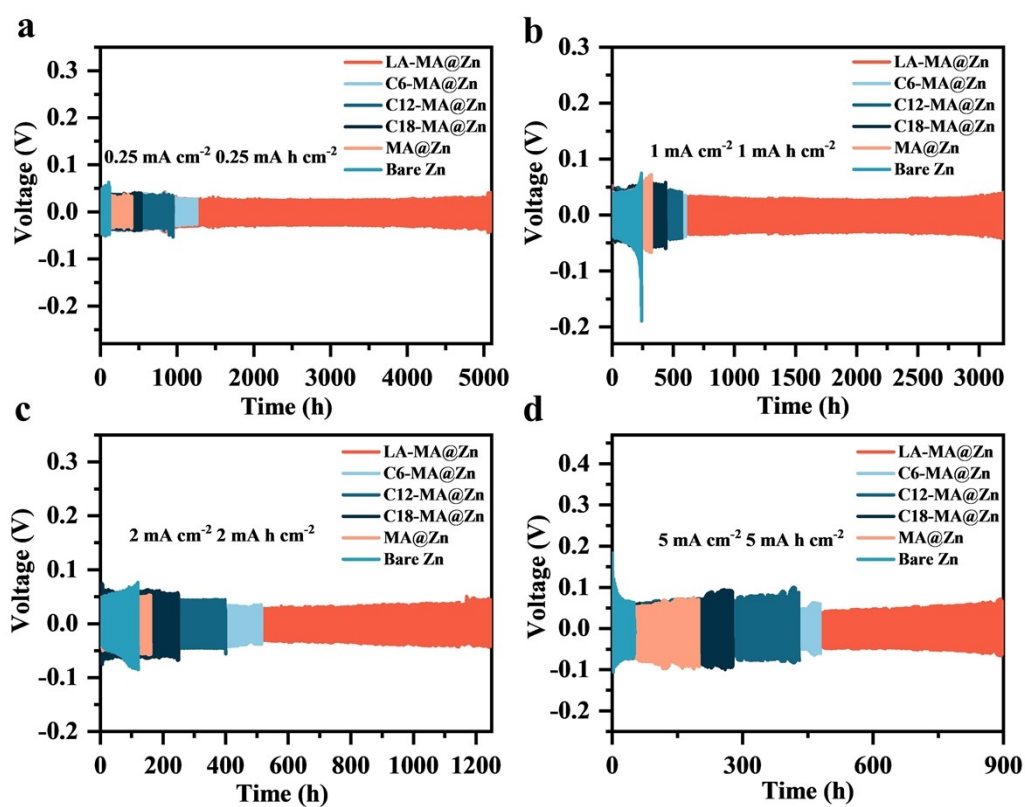
Fig. S6 ν-SO_4^{2-} band of Raman spectroscopy of 2M $ZnSO_4$ solutions in different pore size of mesoporous Al_2O_3.

Fig. S7 Nyquist plots of (a) LA-MA@Zn, (b)bare Zn symmetric cell under different temperatures.

Fig. S8 (a) Linear polarization curves, (b) LSV curves (c) Chronoamperometry curves of LA-MA@Zn and bare Zn.

Fig. S9 The cycling stability of different pore size of mesoporous Al_2O_3 symmetrical cells at current densities of (0.25, 1, 2, and 5 mA cm^{-2}, respectively) and capacities (0.25, 1, 2, and 5 mA h cm^{-2}, respectively).
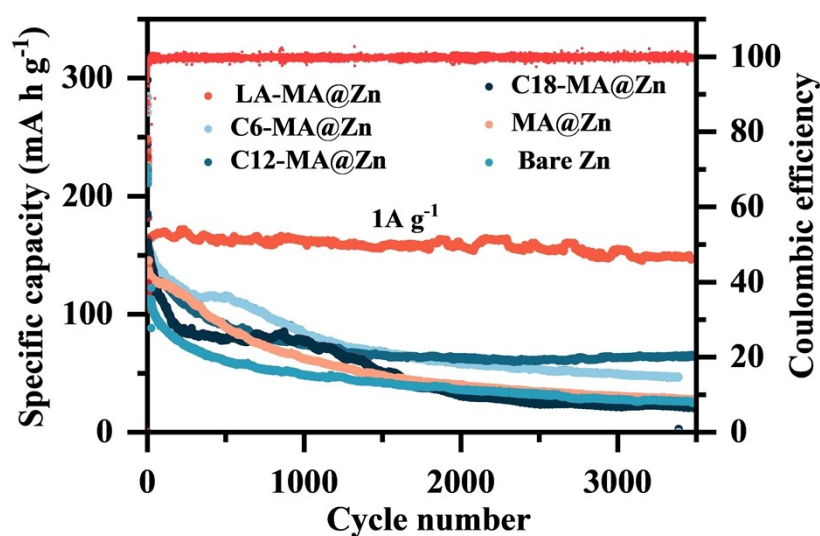
Fig. S10 Long-term cycling performance of different full cells.

Table S1. Electrochemical performance comparison of full-cell in this work and other reported works.

Sample	Current density Capacity	Cycle number	Capacity retention	Reference
LA-MA@Zn‖CNT/MnO$_2$	1 A g^{-1}	Over 3500	94.2%	This work
APTESZn‖ZVO	2 A g^{-1}	600	88.4%	4
ZnO-rich ASEI@Zn‖MnO$_2$	0.5A g^{-1}	1000	70%	5
ZnOMMT-4‖MnO$_2$	2 A g^{-1}	1000	76.7%	6
Zn@PDMS/TiO$_{2-x}$‖MnO$_2$	1C	400	99.4%	7
MCM41- Zn‖K-NVO	1 A g^{-1}	500	74.5%	8
Zn@CaF$_2$‖V$_{10}$O$_{24}$	2 A g^{-1}	1000	70%	9
Zn@TiO$_2$/NC‖MnO$_2$	0.5 A g^{-1}	1000	75%	10
g-C$_3$N$_4$-Zn‖MnO$_2$	1 A g^{-1}	1300	61%	11
V$_2$O$_5$‖ZSM-5‖Zn	1 A g^{-1}	3000	82.67%	12
Zn@PDA-6‖VS$_2$@SS	1 A g^{-1}	1000	81.3%	13
PSPMA@Zn‖MnO$_2$	6C	800	71.5%	14

References

1. B. Naik, V. S. Prasad and N. N. Ghosh, *Journal of Porous Materials*, 2009, **17**, 115-121.

2. Kang, M. Cui, F. Jiang, Y. Gao, H. Luo, J. Liu, W. Liang and C. Zhi, *Advanced Energy Materials*, 2018, **8**, 1801090. 33.

3. H. Yang, Z. Chang, Y. Qiao, H. Deng, X. Mu, P. He and H. Zhou, *Angew Chem Int Ed Engl*, 2020, **59**, 9377-9381.

4. L. Wang, Z. Wang, H. Li, D. Han, X. Li, F. Wang, J. Gao, C. Geng, Z. Zhang and C. Cui, *ACS Nano*, 2023, **17**, 668-677

5. C. Choi, J. B. Park, J. H. Park, S. Yu and D.-W. Kim, *Chemical Engineering Journal*, 2023, **456**, 141015.

6. Y. Wang, Y. Fan, D. Liao, Y. Wu, Y. Yu and C. Hu, *Energy Storage Mater.*, 2022, **51**, 212-222.

7. Z. Guo, L. Fan, C. Zhao, A. Chen, N. Liu, Y. Zhang and N. Zhang, *Adv. Mater.*, 2022, **34**, 2105133.

8. Z. Miao, F. Zhang, H. Zhao, M. Du, H. Li, H. Jiang, W. Li, Y. Sang, H. Liu and S. Wang, *Adv. Funct. Mater.*, 2022, **32**, 2111635.

9. Y. Li, S. Yang, H. Du, Y. Liu, X. Wu, C. Yin, D. Wang, X. Wu, Z. He and X. Wu, *Journal of Materials Chemistry A*, 2022, **10**, 14399-14410.

10. Q. Xu, W. Zhou, T. Xin, Z. Zheng, X. Yuan and J. Liu, *Journal of Materials Chemistry A*, 2022, **10**, 12247-12257.

11. X. Wang, K. Yang, C. Ma, W. Lu, N. Chen, M. Yao, Z. Li, C. Liu, H. Yue, D. Zhang and F. Du, *Chemical Engineering Journal*, 2023, **452**, 139257.

12. J. Zhu, Z. Bie, X. Cai, Z. Jiao, Z. Wang, J. Tao, W. Song and H. J. Fan, *Adv Mater*, 2022, **34**, e2207209.

13. X. Li, M. Wang, H. Wang, Y. Gao, Z. Tang, J. Wang, Y. Feng, Z. Yang, D. Zhou, J. Chen, H. Xie, Y. Huang and X. Li, *ACS Appl Mater Interfaces*, 2022, **14**, 43215-43225.

14. H. Liu, Q. Ye, D. Lei, Z. Hou, W. Hua, H. Yu, N. Li, C. Wei, F. Kang and J.-G. Wang, *Energy & Environmental Science*, 2023, **16**, 1610-1619.